Cite this article
Belletti B, Muttoni A, Ravasini S and Vecchi F
Parametric analysis on punching shear resistance of reinforced-concrete continuous slabs.
Magazine of Concrete Research,
https://doi.org/10.1680/jmacr.18.00123

Research Article
Paper 1800123
Received 12/03/2018; Revised 12/06/2018;
Accepted 12/07/2018

Keywords: punching/slabs & plates/
structural analysis

Magazine of Concrete Research

ice publishing

Parametric analysis on punching shear resistance of reinforced-concrete continuous slabs

Beatrice Belletti
Associate Professor, Department of Engineering and Architecture, University of Parma, Parma, Italy (Orcid:0000-0002-4382-9930)

Aurelio Muttoni
Professor, Ecole Polytechnique Fédérale de Lausanne, Lausanne, Switzerland (Orcid:0000-0001-8418-5556)

Simone Ravasini
Civil Structural Engineer, Department of Engineering and Architecture, University of Parma, Parma, Italy (Orcid:0000-0002-6843-1646)

Francesca Vecchi
PhD Researcher, Department of Engineering and Architecture, University of Parma, Parma, Italy (corresponding author: francesca.vecchi1@studenti.unipr.it) (Orcid:0000-0002-3852-4243)

Punching shear resistance formulations provided by codes are usually calibrated on test results of isolated specimens that typically simulate the slab zone within the points of contraflexure around the column (hogging area). However, the behaviour of actual continuous flat slabs can be different to that of isolated specimens owing to the beneficial contributions of moment redistributions and membrane actions that cannot take place in isolated specimens. This paper presents a parametric study carried out to highlight the influence of the main geometrical features and the reinforcement layout affecting the punching shear resistance of continuous slabs around internal columns.

Notation

a_m	distance between cracks
b_0	length of the control perimeter
c	column size
$[\mathbf{D}_c]$	Jacobian matrix in x, y-coordinate system of concrete
$[\mathbf{D}_s]$	Jacobian matrix in x, y-coordinate system of steel
d	effective depth of the slab
d_g	maximum aggregate size
d_{g0}	reference aggregate size
E_c	modulus of elasticity of concrete
E_s	modulus of elasticity of steel
f_c	concrete compressive strength
f_t	concrete axial tensile strength
f_y	yield strength of the reinforcement steel
G_c	compressive fracture energy of concrete
h	slab thickness
i_n	n-layer of multi-layered element
k_{sys}	coefficient for the performance of punching shear reinforcement systems
L	flat slab span
m_E	average moment per unit length
m_R	average flexural resistance of the slab in the hogging area
r_s	distance between the column axis and the point of contraflexure
S_i	bar spacing
t	finite-element shell thickness
V	acting shear force
V_E	acting shear force
V_R	punching shear resistance
w_{ctu}	maximum crack opening with residual tensile strength
x_i,y_i	direction of the ith order of bar
γ_{xy}	shear strain in the x,y-coordinate system
ε	concrete strain
$\varepsilon_{c,cr}$	concrete strain at maximum compressive stress
$\varepsilon_{c,el}$	elastic compressive strain of concrete
$\varepsilon_{c,pl}$	plastic compressive strain of concrete
$\varepsilon_{c,re}$	experienced minimum compressive strain on the monotonic curve
$\varepsilon_{c,u}$	ultimate strain of concrete in compression
ε_{cr}	cracking of concrete
ε_{sh}	shrinkage strain
ε_{sy}	yielding strain of reinforcement
$\varepsilon_{t,cr}$	concrete strain at maximum tensile stress
$\varepsilon_{t,el}$	elastic tensile strain of concrete
$\varepsilon_{t,pl}$	plastic tensile strain of concrete
$\varepsilon_{t,re}$	experienced minimum tensile strain on the monotonic curve
$\varepsilon_{t,u}$	ultimate tensile strain of concrete
$\varepsilon_{x,y}$	strain along x,y direction, respectively (Figure 2(a))
$\{\boldsymbol{\varepsilon}_c\}$	strain vector of concrete
$\{\boldsymbol{\varepsilon}_{cf}\}$	concrete strain field caused by applied loads
$\{\boldsymbol{\varepsilon}_m\}$	total strain vector of reinforced-concrete element
$\{\boldsymbol{\varepsilon}_s\}$	strain vector of steel
$\{\boldsymbol{\varepsilon}_{sf}\}$	steel strain field caused by applied loads
$\{\boldsymbol{\varepsilon}_{sh}\}$	shrinkage strain
ρ_{hogg}	percentage of hogging reinforcement
ρ_{sagg}	percentage of sagging reinforcement
σ	total stress field of reinforced-concrete member
σ_c	stress field of concrete
$\sigma_{cl,cr}$	residual bond stress
σ_s	stress field of steel

σ_{rad}	radial stresses
σ_{tang}	tangential stresses
$\sigma_{x,y}$	stress along x,y direction, respectively (Figure 2(a))
θ_i	angle between the direction of the ith order of bars and the x-direction
τ_{xy}	shear stress in the x,y-coordinate system
Ψ	slab rotation
Ψ_R	ultimate rotation corresponding to the punching shear resistance

Introduction

Reinforced-concrete (RC) flat slabs are common structural solutions in residential and multi-storey buildings. The behaviour of RC flat slabs can be governed at failure by punching shear close to columns. Most of the code formulations for punching shear strength assessment (ACI 318-14 (ACI, 2014); Eurocode 2 (CEN, 2004); fib Model Code 2010 (fib, 2013)) are based or calibrated on experimental tests usually carried out on isolated specimens. Nevertheless, the bending and the shear resistance of isolated specimens can be lower than the resistance of actual continuous RC flat slabs due to moment redistribution and compressive membrane action (CMA) or tensile membrane action (TMA) effects (Figure 1).

CMA and TMA effects can be considered in the capacity assessment of restrained slabs (Arshian and Morgenthal, 2017), continuous RC (Amir *et al.*, 2016; Foster *et al.*, 2004; Ladner *et al.*, 1977) and steel fibre-reinforced concrete (SFRC) slabs (Di Prisco *et al.*, 2016), bridge deck slabs (Kirkpatrick *et al.*, 1986; Taylor *et al.*, 2007), slabs subjected to large displacement due to fire (Bailey, 2001), slabs subjected to a sudden removal of a supporting column (Dat and Hai, 2013; Gouverneur *et al.*, 2013a; Qian *et al.*, 2015) and slabs subjected to deterioration (Botte *et al.*, 2014). CMA or TMA effects can be evaluated using yield line methods (Bailey, 2001; Burgess, 2017; Dat and Hai, 2013; Gouverneur *et al.*, 2013a; Qian *et al.*, 2015), rigid plastic approach (Park and Gamble, 2000; Rankin and Long, 1997; Wood, 1961) for RC, SFRC and strengthened fibre-reinforced polymer (FRP) members (Zeng *et al.*, 2016), sector models based on axisymmetric assumptions (Einpaul *et al.*, 2015, 2016) and finite-element methods (Belletti *et al.*, 2016; Soares and Vollum, 2015). Membrane action effects on continuous slabs have been recently analysed using nonlinear finite-element analysis (NLFEA) and different modelling approaches, for example using three-dimensional (3D) hexahedral elements (Genikomsou and Polak, 2017) or multi-layered shell elements (Cantone *et al.*, 2016). In this paper, the shrinkage effects on concrete cracking and on the punching shear resistance are studied. This aspect could be significant for the structural assessment of existing structures carried out using refined numerical tools, such as NLFEA methods, which are able to take into account hidden resistance capacities, but are less conservative than analytical approaches (Belletti *et al.*, 2015a, 2015b).

To this aim, a parametric study has been carried out to investigate the dependency of membrane action and moment redistribution on the geometrical features and reinforcement layout of continuous slabs. Therefore, different values of base column dimension, slab thickness (with constant value of the effective depth, which means that the influence of reinforcement cover of the tensile reinforcement is investigated), slab span and ratios of hogging and sagging reinforcement have been considered. This work focuses on the region of the slab supported on internal columns without openings, where the highest influence of CMA may be expected. The activation of CMA in edge and corner columns, as well as internal columns with openings, requires further research that is out of the scope of this work.

The parametric study was carried out using NLFEA performed using a multi-layered shell model and PARC_CL 2.0 (physical approach for reinforced concrete for cyclic loading) crack model implemented in the user-defined material model (UMAT) subroutine for Abaqus Code. The numerical results are then post-processed using the critical shear crack theory (CSCT)

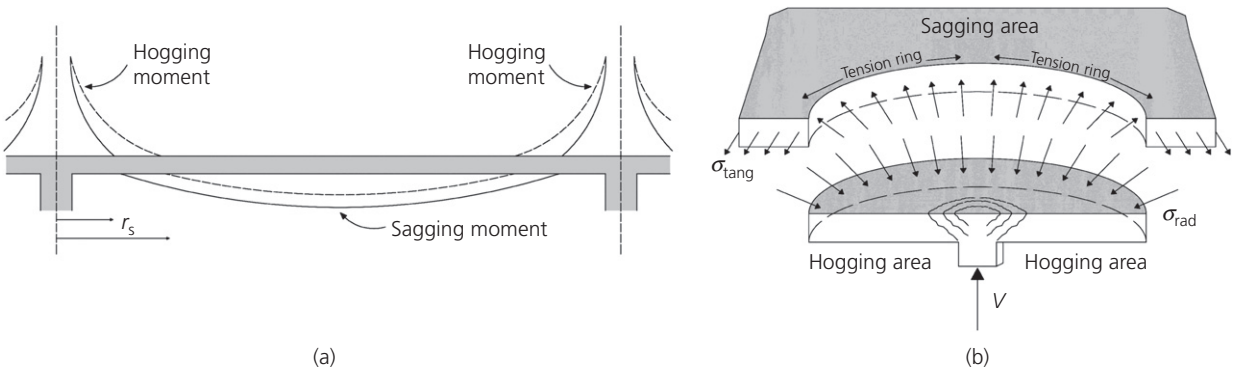

Figure 1. (a) Moment redistribution between hogging and sagging areas; (b) CMA – radial and tangential stresses (σ_{rad} and σ_{tang}) and effect of the tension ring on the hogging area

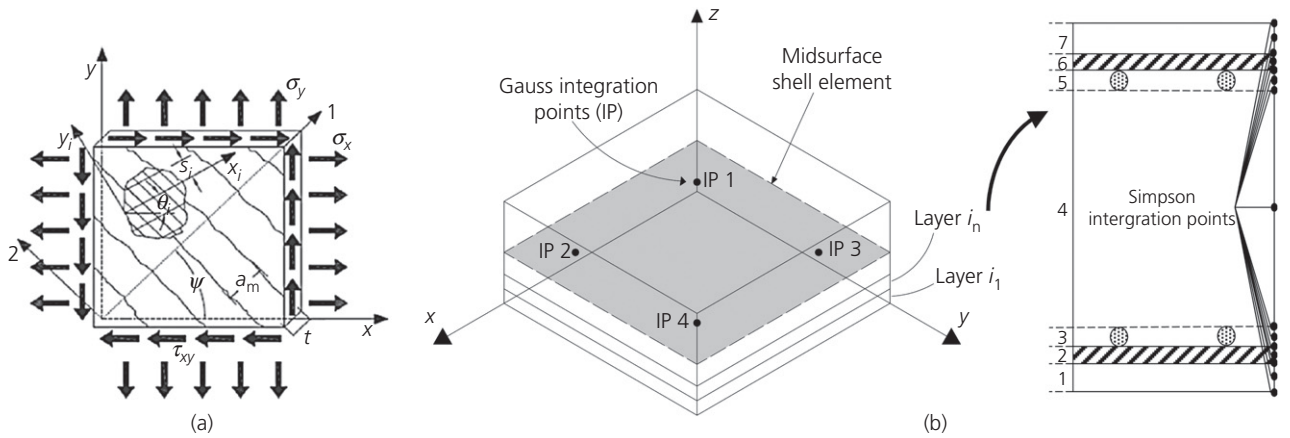

Figure 2. (a) PARC_CL 2.0 crack model; (b) multi-layered shell approach

failure criterion to obtain the punching shear resistance (as performed by Belletti *et al.* (2015a, 2015b), Shu *et al.* (2017) and Soares and Vollum (2015, 2016)). The effect of shrinkage is considered in this work on the slab response (e.g. load–rotation relationship), and its influence on the failure criterion is neglected. The effect of creep on both slab response and shear strength is usually neglected according to the CSCT, since the effect of the increased rotation is assumed to be compensated for by the increased local resistance.

In the framework of the level of approximation (LoA) approach, the punching shear resistance estimated using NLFEA (LoA IV) is compared with the resistances analytically obtained using LoA II and LoA III. These latter comparisons have been carried out with and without considering membrane action and moment redistribution effects detected using NLFEA as a function of the slab rotation.

Multi-layered shell modelling, PARC_CL 2.0 crack model and CSCT failure criterion

NLFEA is carried out using multi-layered shell elements and the PARC_CL 2.0 crack model (Belletti *et al.*, 2017) implemented in Abaqus as a user subroutine. PARC_CL 2.0 crack model is a new release of previous models (PARC for monotonic loading (Belletti *et al.*, 2001) and PARC_CL 1.0 for secant unloading (Belletti *et al.*, 2013)), which is able to account for hysteretic loops and plastic deformations in the case of cyclic loading. PARC_CL 2.0 is total strain fixed, meaning that after cracking, the 1,2-coordinate system remains fixed at the integration point, Figure 2(a). The reinforcement is assumed to be smeared in the hosting concrete elements. Nonlinear stress–strain relationships for concrete and steel, multiaxial state of stress for concrete and aggregate interlock are considered. Since the PARC_CL 2.0 crack model is suitable for a plane stress state, the thickness of the slab is subdivided into layers. Four Gauss integration points in the plane of the shell and three Simpson integration points in the thickness of each layer have been adopted (Figure 2(b)). The geometric nonlinearity, which has to be set to evaluate membrane actions, is considered by adopting a Lagrangian formulation.

Since the adopted multi-layered shell elements are not able to predict the nonlinear behaviour over the thickness of the slab, a post-processing approach, as presented in (Belletti *et al.*, 2015a, 2015b), is used on the basis of the CSCT (Muttoni, 2008). The CSCT failure criterion enables the prediction of the punching shear resistance of a slab subjected to a concentrated load depending on the maximum slab rotation Ψ (Figure 3). The punching shear capacity depends on the opening width of the critical shear crack, which is associated to the product Ψd and the aggregate interlock across the inclined crack (Figure 3(a)).

The failure criterion given in Equation 1 is derived from a mechanical model presented in Guidotti (2010), Muttoni (2008), Muttoni *et al.* (2018) and Simões *et al.* (2018).

$$1. \qquad V_{\mathrm{R}}(\psi) = \frac{(3/4) b_0 d \sqrt{f_{\mathrm{c}}}}{1 + 15\left(\psi d / \left(d_{\mathrm{g}} + d_{\mathrm{g0}}\right)\right)}$$

where b_0 is the length of the control perimeter at a distance $0{\cdot}5d$ from the column edge, Figure 3(b), d is the effective depth of the slab, d_{g} is the maximum aggregate size, d_{g0} is the reference aggregate size (16 mm) and f_{c} is the concrete compressive strength in MPa.

The slab rotation Ψ proposed by fib Model Code 2010 (fib, 2013) for LoA II is

$$2. \qquad \psi = 1{\cdot}5 \frac{r_{\mathrm{s}}}{d} \frac{f_{\mathrm{y}}}{E_{\mathrm{s}}} \left(\frac{m_{\mathrm{E}}}{m_{\mathrm{R}}}\right)^{1{\cdot}5}$$

where r_{s} is the distance between the column axis and the point of contraflexure, f_{y} is the yield strength of the reinforcement

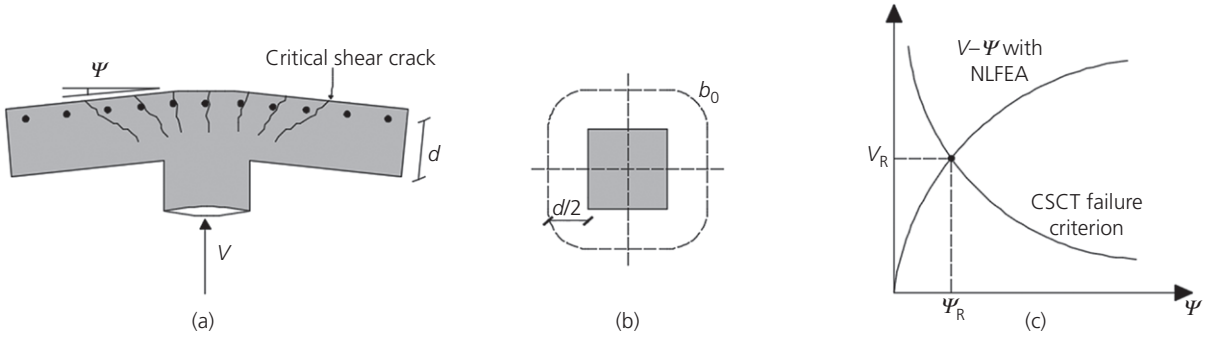

Figure 3. (a) Punching shear strength correlated to the crack opening; (b) assumption of control perimeter at 0·5*d* from the edge of the column; (c) punching shear resistance at the intersection between nonlinear load–rotation curve and CSCT failure criterion

steel, E_s is its modulus of elasticity, m_E is the average moment per unit length for calculation of the flexural reinforcement in hogging area and m_R is the average flexural resistance of the slab in the hogging area.

For LoA I, it is assumed that the flexural reinforcement in the hogging area is fully plasticised, so that rotation Ψ may be calculated assuming $m_E/m_R = 1$ in Equation 2. According to fib Model Code 2010, this is the first step to verify whether punching or flexure is governing and is thus not comparable to calculations presented in this paper.

For the LoA II, m_E is estimated on the basis of the acting shear force V_E ($m_E = V_E/8$ for an interior symmetric column). This allows a straightforward design, but needs an iteration until $V_E = V_R$ for calculating the punching shear resistance (the punching shear resistance corresponds to the intersection point between the failure criterion of Equation 1 and the load–rotation relationship of Equation 2) (Figure 3(c)).

In the LoA III, linear finite-element analyses can be used for a better estimation of the radius r_s and of the acting moment m_E. In this case, the coefficient 1·5 in Equation 2 is replaced by 1·2.

For LoA IV, the load–rotation relationship in Equation 2 is replaced by a relationship determined using NLFEA. Additionally, in this case, the punching shear resistance V_R corresponds to the intersection point between the NLFEA load–rotation curve and the failure criterion (Figure 3(c)). The adopted procedure has been validated by comparing NLFEA results with experimental observations in Cantone *et al.* (2016), Muttoni (2008) and Belletti *et al.* (2015a, 2015b). Furthermore, for some selected case studies, in Shu *et al.* (2017) the shear punching resistances obtained using shell modelling and PARC_CL 2.0 crack model have been compared with shear punching resistances obtained using brick modelling and a crack model implemented in DIANA material library (Manie and Kikstra, 2010). In Shu *et al.* (2017) it is highlighted that the effectiveness of shell element modelling prediction of punching shear resistance is comparable with results obtained using brick element modelling. Furthermore, slab modelling requires less time and memory compared to brick element modelling, whose NLFEA results are more mesh- and material parameter-dependent.

Moment redistribution, membrane action and shrinkage effects

Significant hidden resistance reserves of continuous RC slabs can be provided by moment redistribution due to nonlinear behaviour and by membrane action. These beneficial effects cannot be observed in the conventional experiments performed on isolated RC flat slabs, but can be evaluated via onerous experimental tests (Gouverneur *et al.*, 2013b; Ladner *et al.*, 1977) on continuous flat slabs or by NLFEA simulations (Botte *et al.*, 2016; Genikomsou and Polak, 2017).

Membrane actions are strongly correlated to the boundary conditions of the slab. In the present study, two different static cases are investigated.

(*a*) Isolated slab reproducing the hogging area of a flat slab without CMA, having dimension equal to 0·22*L*, and subjected to concentrated loads corresponding to the typical experimental setup (Figure 4(b)).
(*b*) Self-confined continuous flat slab having regular spans *L* loaded with a uniform pressure to simulate permanent and variable loads (Figure 4(a)).

Owing to the symmetry of loading and boundary conditions, a quarter of the isolated and self-confined slab is considered (Figure 4).

Influence of membrane action

The lateral expansion of the cracked concrete in the hogging area is restrained by the outer part of the slab and this leads to the formation of radial and tangential stresses. Radial compressive membrane stresses in the column area (so-called CMA) are in equilibrium with a tangential tension ring in the outer area of the slab (Figure 1(b)). This phenomenon increases stiffness

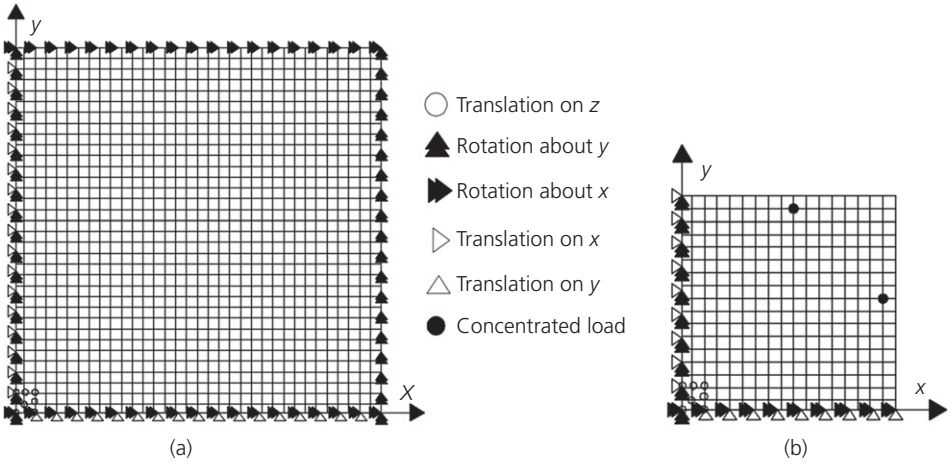

Figure 4. Boundary conditions for: (a) self-confined slab – pressure; (b) isolated slab – concentrated loads

and strength of flat slabs (compared to isolated specimens or flat slabs where CMA is negligible) (Belletti *et al.*, 2015a, 2015b; Einpaul *et al.*, 2015, 2016; Soares and Vollum, 2015). The potential beneficial influence of CMA on the failure criterion (Clément *et al.*, 2014) is not addressed in the present study.

Influence of moment redistribution

For calculating the punching shear resistance of RC flat slabs according to fib Model Code 2010 (LoA II and III), it may be assumed that the position of the point of contraflexure (radius r_s) is constant and is not affected by cracking or yielding of the reinforcement (in the case of flat slabs with regular spans and column sizes, it may be assumed that $r_s \approx 0{\cdot}22L$ according to linear elastic calculations). Actually, both cracking of concrete and yielding of reinforcement in the hogging area cause moment redistributions that lead to a reduction of the radius r_s (if the stiffness of the hogging area is reduced, the point of contraflexure moves toward the column), so that the punching shear resistance is increased (as rotation Ψ according to Equation 2 is reduced). In contrast, cracking and yielding in the sagging area lead to an increase of radius r_s (and eventually to a reduction of the punching shear resistance). As cracking and yielding are more pronounced in the hogging area (at least for usual column sizes and reinforcement ratios), accounting for moment redistribution usually leads to an increase of the punching shear resistance (Einpaul *et al.*, 2015, 2016).

Shrinkage

In an unsaturated environment, shrinkage generates a contraction of concrete volume that develops with time. Since concrete contraction is restrained by the presence of reinforcement, shrinkage can facilitate cracking; thus the tension ring around the column is less effective and membrane actions are reduced.

The shrinkage effect in the PARC_CL 2.0 model is simplified considering an average deformation, without resolving the solution of thermo-hygrometric problems and neglecting temporal and spatial evolution of the phenomenon. Therefore, the model is able to capture the shrinkage effects on strains and critical load (Wu and Gilbert, 2008). In the parametric study carried out and presented in the present study, a constant shrinkage strain ε_{sh} of 3×10^{-4} is considered. In the PARC_CL 2.0 crack model, shrinkage is applied as an additional tensile strain (Equation 3) (Bernardi *et al.*, 2016).

$$\{\boldsymbol{\varepsilon}_{sh}\} = \begin{Bmatrix} \varepsilon_{sh} \\ \varepsilon_{sh} \\ 0 \end{Bmatrix} \tag{3}$$

PARC_CL 2.0 is a crack model (Belletti *et al.*, 2017) that assumes perfect bond condition between concrete and steel; for this reason, the strain field of the RC element $\{\boldsymbol{\varepsilon}_m\}$ is given by Equation 4

$$\{\boldsymbol{\varepsilon}_m\} = \{\boldsymbol{\varepsilon}_c\} = \{\boldsymbol{\varepsilon}_s\} = \begin{Bmatrix} \varepsilon_x \\ \varepsilon_y \\ \gamma_{xy} \end{Bmatrix} \tag{4}$$

where $\{\boldsymbol{\varepsilon}_c\}$ is the strain vector of concrete and $\{\boldsymbol{\varepsilon}_s\}$ is the strain vector of steel.

Therefore, the linear elastic uncracked response is modelled by including the free shrinkage strain $\{\boldsymbol{\varepsilon}_{sh}\}$ of the concrete in the total concrete strain field (Equation 5).

$$\{\boldsymbol{\varepsilon}_m\} = \{\boldsymbol{\varepsilon}_c\} = \{\boldsymbol{\varepsilon}_{cf}\} - \{\boldsymbol{\varepsilon}_{sh}\} \tag{5}$$

where $\{\boldsymbol{\varepsilon}_{cf}\}$ is the concrete strain field caused by stress, while for the steel reinforcement the total strain is given by Equation 6.

$$\{\boldsymbol{\varepsilon}_m\} = \{\boldsymbol{\varepsilon}_s\} = \{\boldsymbol{\varepsilon}_{sf}\} \tag{6}$$

where $\{\boldsymbol{\varepsilon}_{sf}\}$ is the steel strain field caused by stress.

Consequently, the resultant stress fields in concrete and steel are given respectively by Equations 7 and 8, while the total stress field in RC member is given by Equation 9

7. $$\{\boldsymbol{\sigma}_c\} = [\mathbf{D}_c]\{\boldsymbol{\varepsilon}_{cf}\} = [\mathbf{D}_c](\{\boldsymbol{\varepsilon}_c\} + \{\boldsymbol{\varepsilon}_{sh}\})$$

8. $$\{\boldsymbol{\sigma}_s\} = [\mathbf{D}_s]\{\boldsymbol{\varepsilon}_{sf}\}$$

Table 1. Mechanical properties of steel and concrete

f_c: MPa	E_c: MPa	f_y: MPa	E_s: MPa
35	32 600	520	200 000

9. $$\{\boldsymbol{\sigma}\} = \{\boldsymbol{\sigma}_c\} + \{\boldsymbol{\sigma}_s\} = [\mathbf{D}_c](\{\boldsymbol{\varepsilon}_c\} + \{\boldsymbol{\varepsilon}_{sh}\}) + [\mathbf{D}_s]\{\boldsymbol{\varepsilon}_s\}$$

where $[\mathbf{D}_c]$ and $[\mathbf{D}_s]$ are the Jacobian matrix in x, y-coordinate system of concrete and steel bars, respectively, which can be found in Belletti *et al.* (2017).

Parametric study of continuous slabs

Geometrical and mechanical properties

In this paper, a parametric analysis has been carried out to study the influence of several parameters on the punching resistance of RC continuous slabs, namely hogging and sagging

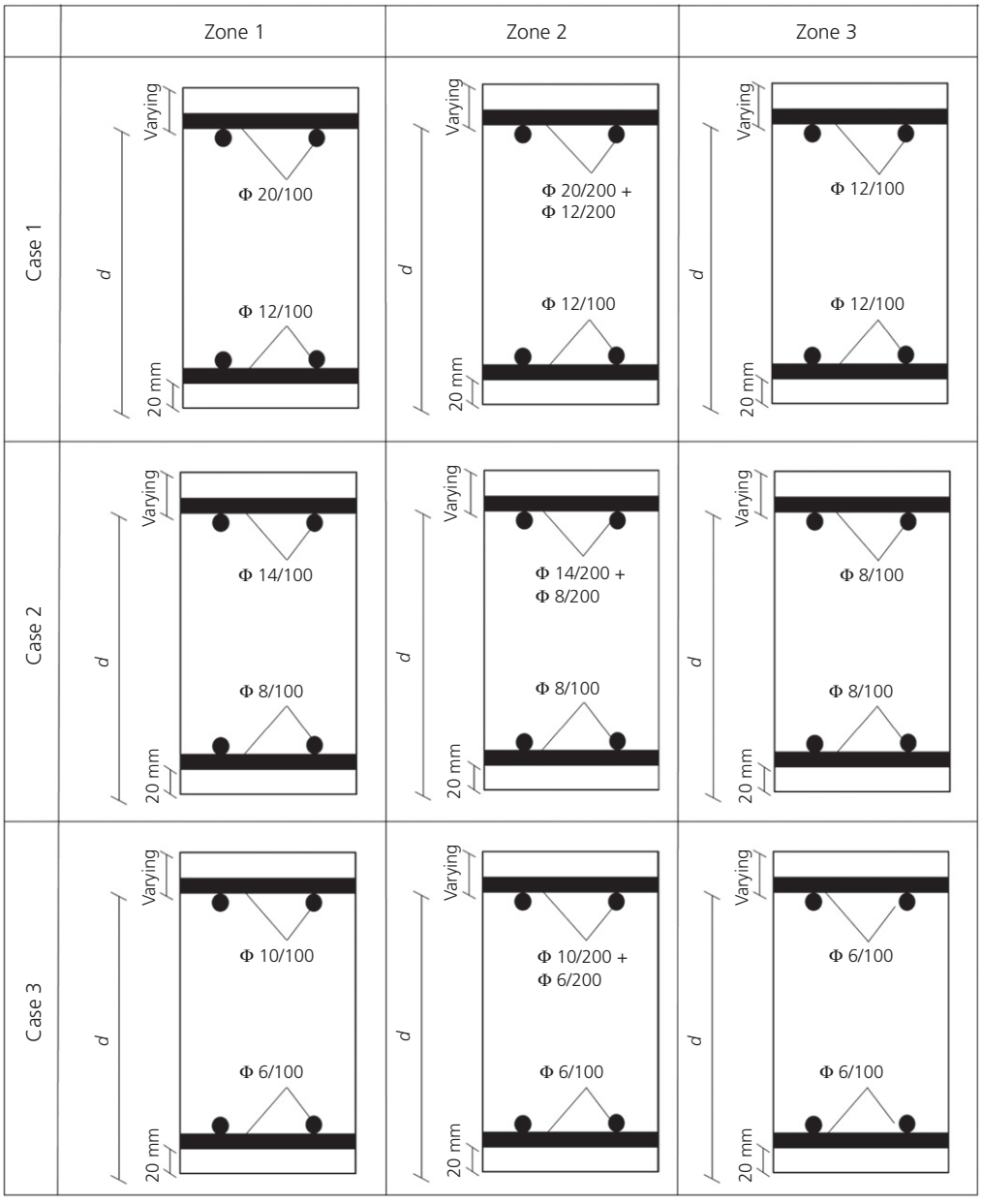

Figure 5. Reinforcement layout for each case study

reinforcement ratios, geometrical properties of the slab and shrinkage effect.

The mechanical properties for concrete and steel are kept constant for all the analyses (Table 1).

The parametric analysis is carried out by varying the column size c, the flat slab span L, the slab thickness h (the effective depth is kept constant, $d = 210$ mm for all the analyses, which means that, in fact, the cover of the tensile reinforcement has been varied (Figure 5)) and the percentage of hogging and sagging reinforcement, ρ_{hogg} and ρ_{sagg}, respectively. Table 2 summarises the investigated values for the parametric study, which lead to 360 combinations and NLFEA.

Table 2. Geometrical properties of RC flat slabs for parametric analyses

c: mm	h: mm	L: m	d: mm
130	230	4	210
195	250	5	
260	270	6	
325	290	7	
390	310	8	

Table 3. Reinforcement steel ratios for each case of study

	Case 1	Case 2	Case 3
Zone 1: $0{\cdot}4L \times 0{\cdot}4L$ around column	$\rho_{hogg} = 1{\cdot}5\%$ $\rho_{hogg}/\rho_{sagg} = 3$ $\rho_{sagg} = 0{\cdot}5\%$	$\rho_{hogg} = 0{\cdot}75\%$ $\rho_{hogg}/\rho_{sagg} = 3$ $\rho_{sagg} = 0{\cdot}25\%$	$\rho_{hogg} = 0{\cdot}375\%$ $\rho_{hogg}/\rho_{sagg} = 3$ $\rho_{sagg} = 0{\cdot}125\%$
Zone 2: support strips outside Zone 1	$\rho_{sagg} = 0{\cdot}5\%$ $\rho_{hogg}/\rho_{sagg} = 2$ $\rho_{hogg} = 1\%$	$\rho_{sagg} = 0{\cdot}25\%$ $\rho_{hogg}/\rho_{sagg} = 2$ $\rho_{hogg} = 0{\cdot}5\%$	$\rho_{sagg} = 0{\cdot}125\%$ $\rho_{hogg}/\rho_{sagg} = 2$ $\rho_{hogg} = 0{\cdot}25\%$
Zone 3: central part of the span	$\rho_{sagg} = 0{\cdot}5\%$ $\rho_{hogg}/\rho_{sagg} = 1$ $\rho_{hogg} = 0{\cdot}5\%$	$\rho_{sagg} = 0{\cdot}25\%$ $\rho_{hogg}/\rho_{sagg} = 1$ $\rho_{hogg} = 0{\cdot}25\%$	$\rho_{sagg} = 0{\cdot}125\%$ $\rho_{hogg}/\rho_{sagg} = 1$ $\rho_{hogg} = 0{\cdot}125\%$

Three cases with three hogging reinforcement ratios in the column area ($0{\cdot}4L \times 0{\cdot}4L$) are studied: $\rho_{hogg} = 1{\cdot}5\%$, $0{\cdot}75\%$, $0{\cdot}375\%$. For all cases, the sagging reinforcement is uniformly distributed over the span with a reinforcement ratio $\rho_{sagg} = \rho_{hogg}/3$ (Zone 1) and the hogging reinforcement is reduced to 2/3 and 1/3 in the support strips outside the column area (Zone 2) and the central part of the span (Zone 3), respectively (Table 3 and Figure 6).

The shear reinforcement leads to an increment of the punching shear resistance owing to the beneficial limitation of the critical shear crack width. The presence of shear reinforcement could be taken into account by adding its strength to the basic failure criterion, for which only the concrete contribution is considered. The maximum punching shear resistance is limited by crushing of the concrete struts in the supported area and it is achieved by using a value of $k_{sys} = 2{\cdot}8$ for studs (diameters of heads larger or equal to three-times the bar diameter) (fib, 2013).

Punching shear resistance dependency on parameters

In Figure 7, the load–rotation curves for the self-confined continuous flat slab and the isolated specimen are shown. The punching shear resistance corresponds to the intersection of the load–rotation curves with the CSCT failure criterion. It can be observed that the response of continuous slabs is stiffer than the response of isolated specimens, leading to higher punching shear resistances. In addition, the difference between

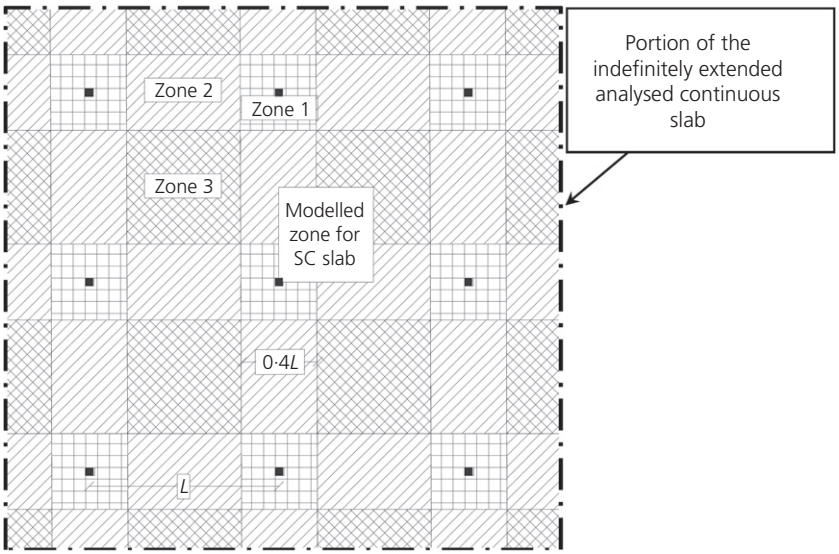

Figure 6. Zone subdivision for the analysed continuous slab (SC, self-confined)

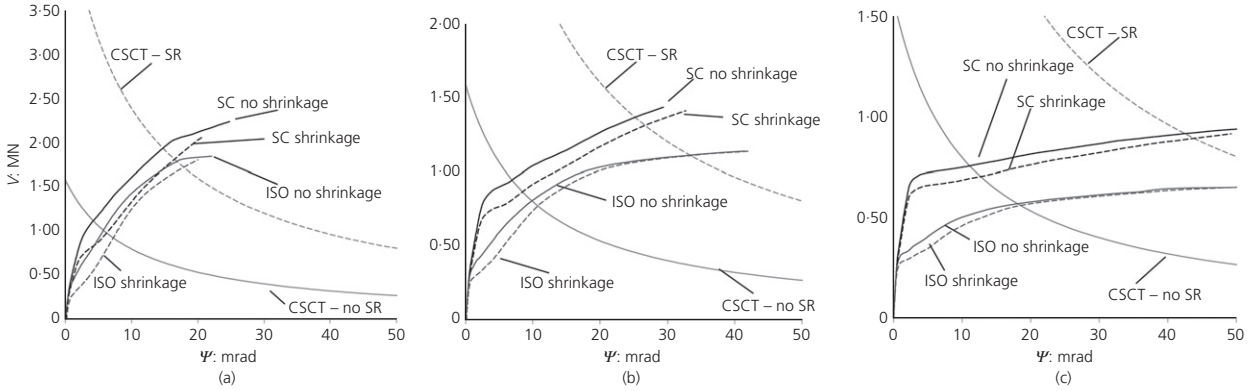

Figure 7. Load–rotation curves against CSCT failure criterion for: (a) $\rho_{hogg} = 1{\cdot}5\%$; (b) $\rho_{hogg} = 0{\cdot}75\%$; (c) $\rho_{hogg} = 0{\cdot}375\%$ (ISO, isolated specimen; SC, self-confined; SR, shear reinforcement)

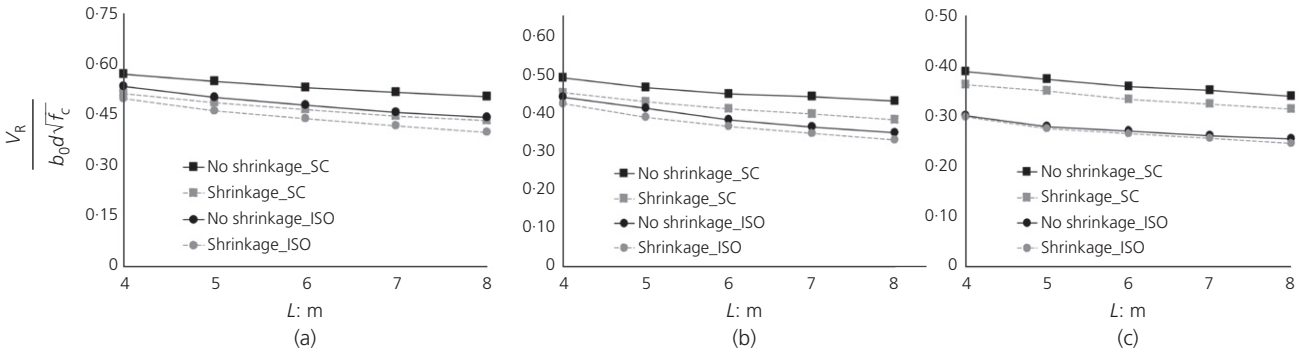

Figure 8. Normalised punching shear resistance (in $(MPa)^{1/2}$) as a function of span L: (a) $\rho_{hogg} = 1{\cdot}5\%$; (b) $\rho_{hogg} = 0{\cdot}75\%$; (c) $\rho_{hogg} = 0{\cdot}375\%$ (case with $c = 260$ mm, $h = 250$ mm) (ISO, isolated specimen; SC, self-confined)

continuous and isolated slab response predictions increases when the hogging reinforcement decreases.

It is well known that membrane actions are strongly dependent on the boundary condition of the RC flat slab, but Figure 7 shows that membrane actions can also have non-negligible effects in the case of self-confined slabs without considering horizontal restraints provided by vertical supports (such as columns, walls etc.).

To evaluate the difference between flat slabs without and with shear reinforcement, the failure criterion associated to shear reinforcement is also considered in Figure 7 (maximum shear resistance with $k_{sys} = 2{\cdot}8$ for stud shear reinforcement according to fib Model Code 2010). As expected, the failure mode can change considering the isolated or the self-confined slabs. For example, in the case of $\rho_{hogg} = 0{\cdot}375\%$ (Figure 7(c)), the isolated slabs fail due to bending while the continuous slabs fail in a mix mode due to punching shear reached after partial yielding of hogging and sagging reinforcement. Figure 7 also shows the influence of concrete shrinkage on the punching shear resistance. Since shrinkage causes anticipated cracking, its effects on punching shear resistance are more evident in cases of high values of hogging reinforcement ratio (Figure 7(a), where $\rho_{hogg} = 1{\cdot}5\%$), while they can be considered negligible in cases of low values of hogging reinforcement ratio (Figure 7(c), where $\rho_{hogg} = 0{\cdot}375\%$). This can be explained by the fact that in cases of low reinforcement ratios, punching shear resistance is reached after extensive yielding in hogging and sagging areas where the effect of shrinkage almost disappears.

Figure 8 shows the normalised punching shear resistances as a function of the slab span L for the case without shear reinforcement; the punching shear resistance diminishes as the span increases because the slab rotation Ψ increases. The punching shear resistance of isolated slabs is similar to the punching shear resistance of continuous slabs calculated considering the shrinkage effect for $\rho_{hogg} = 1{\cdot}5\%$. In contrast, the prediction of the punching shear resistance of continuous slabs is higher than the punching shear resistance of isolated slabs for lower hogging reinforcement ratio values, also considering shrinkage effects.

In Figure 9, the influence of column size c is shown for the case without shear reinforcement. It can be noted that the

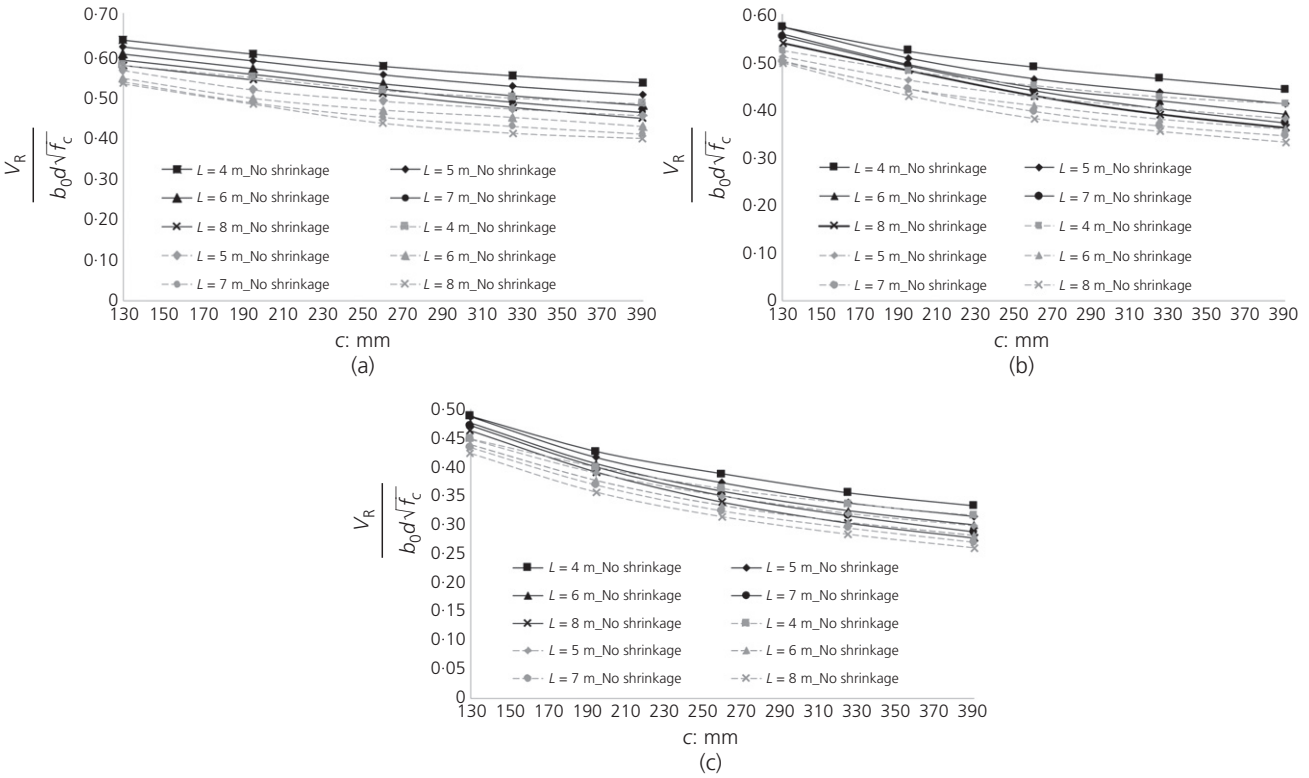

Figure 9. Influence of column size c on the normalised punching shear resistance (in $(MPa)^{1/2}$): (a) $\rho_{hogg} = 1{\cdot}5\%$; (b) $\rho_{hogg} = 0{\cdot}75\%$; (c) $\rho_{hogg} = 0{\cdot}375\%$

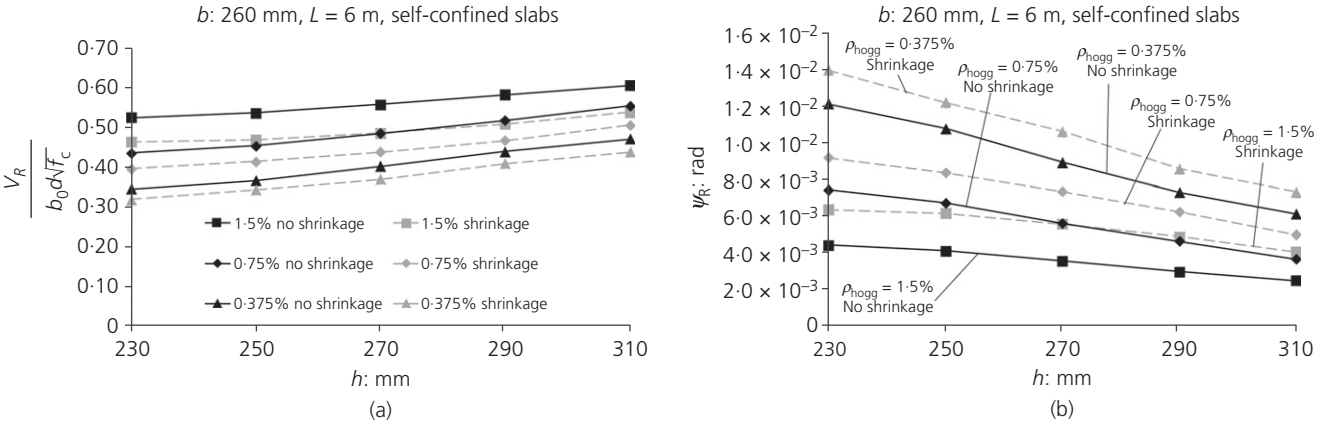

Figure 10. Punching shear resistance (in $(MPa)^{1/2}$) (a) and rotation (b) with variation of thickness h of slab (case with $c = 260$ mm, $d = 210$ mm, $L = 6$ m)

dimensionless punching shear resistance reduces as the column size increases because, keeping fixed all the other parameters, the rotation of the slab increases.

Figure 10 shows the influence of the slab thickness h on the normalised punching shear resistance (the effective depth $d = 210$ mm is kept constant) for the case without shear reinforcement. For the isolated specimen, the punching shear resistance is constant as in the model it is assumed that the reinforcement cover on the tensile side has no influence on the shear resistance. Conversely, for continuous flat slabs, the total slab thickness has a non-negligible effect on the load-carrying capacity as the tensile ring around the column can also develop in the cover above the upper reinforcement. It must be

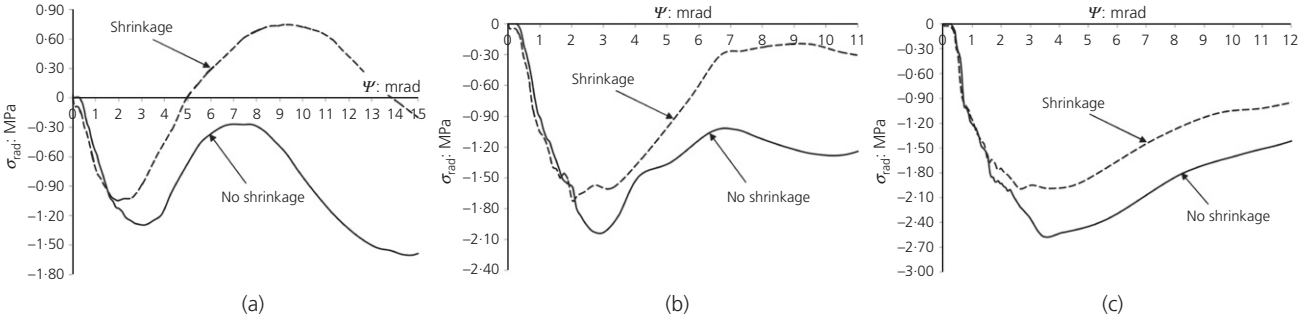

Figure 11. Difference in radial stress with and without shrinkage effect for (a) $\rho_{hogg} = 1{\cdot}5\%$; (b) $\rho_{hogg} = 0{\cdot}75\%$; (c) $\rho_{hogg} = 0{\cdot}375\%$ (case with $c = 260$ mm, $h = 250$ mm, $L = 6$ m, compressive stress negative)

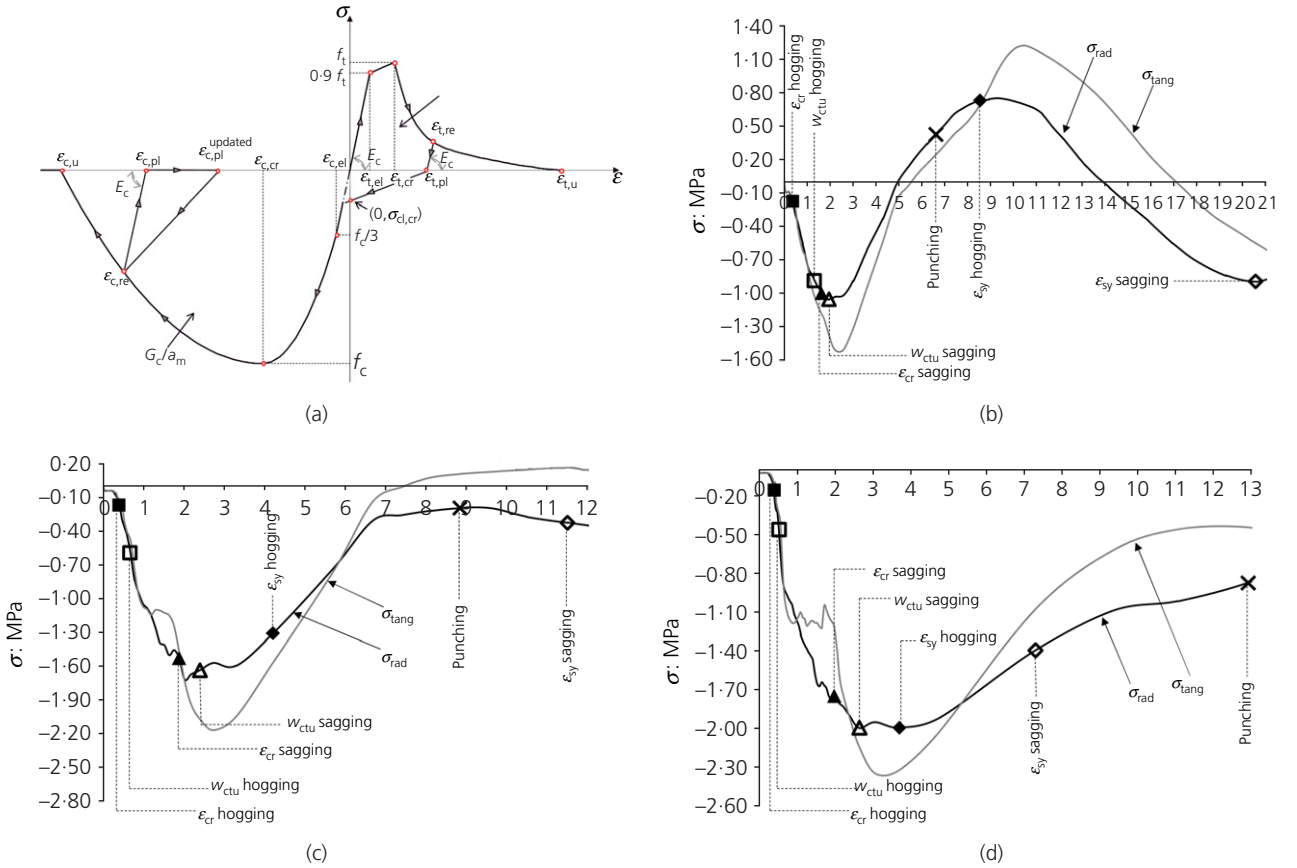

Figure 12. (a) Stress–strain diagram assumed for concrete. Radial and tangential stresses considering shrinkage effect: (b) $\rho_{hogg} = 1{\cdot}5\%$; (c) $\rho_{hogg} = 0{\cdot}75\%$; (d) $\rho_{hogg} = 0{\cdot}375\%$ (case $c = 260$ mm, $h = 250$ mm, $L = 6$ m, compressive stress negative)

noted that this effect is neglected in codes of practice as they are based or calibrated on tests with isolated slab specimens.

Membrane actions in continuous slabs

The average values of radial stresses σ_{rad} and tangential stresses σ_{tang} over the control perimeter b_0 at distance $0{\cdot}5d$ from the edge of the column have been calculated using NLFEA on continuous slabs. In Figures 11 and 12, radial stresses σ_{rad} and tangential stresses σ_{tang} are reported as a function of the slab rotation Ψ for the case with $c = 260$ mm, $h = 250$ mm, $d = 210$ mm and $L = 6$ m. In Figure 11, it is possible to appreciate the effect of shrinkage on the radial stress for the three selected hogging reinforcement ratios ρ_{hogg}. As expected, the concrete shrinkage leads to a reduction of radial stress σ_{rad}. Comparing Figures 11(a)–11(c), it is worth noting that the first peak of the

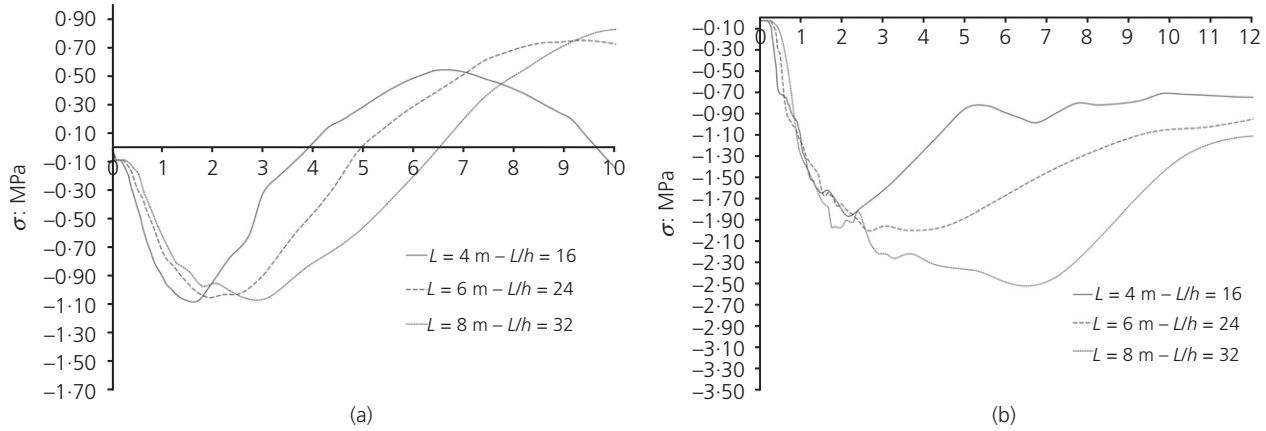

Figure 13. Influence of the slab slenderness on the development of membrane actions for (a) $\rho_{hogg} = 1{\cdot}5\%$; (b) $\rho_{hogg} = 0{\cdot}375\%$ (case $c = 260$ mm, $h = 250$ mm)

radial stress σ_{rad} increases as the hogging reinforcement ratio ρ_{hogg} decreases. This effect is due to the higher difference between the stiffness in hogging and sagging zones registered in the case of low hogging reinforcement ratios; furthermore, higher compressive resultant stresses are observed in cases of lower reinforcement ratios as the slab rotation Ψ is increasing.

Figure 12 shows both radial and tangential stresses (σ_{rad} and σ_{tang}) for the continuous flat slab with concrete shrinkage. The most interesting strain limits are marked as follows: cracking of concrete (corresponding to ε_{cr}, see also Figure 12(a)); maximum crack opening with residual tensile strength (corresponding to w_{ctu}, see Figure 12(a), calculated as $w_{ctu} = \varepsilon_{t,u} \times a_m$, where a_m is the distance between cracks; see Belletti *et al.* (2017)); and yielding strain of reinforcement (ε_{sy}). It can be seen from Figures 12(b)–12(d), that the peak value of radial stresses σ_{rad} corresponds to the achievement of the residual tensile strength of concrete (crack opening w_{ctu}) in the sagging area, which corresponds to the maximum ring effect for self-confined slabs. Depending on the intersection with the CSCT failure criterion, punching shear failure occurs before yielding of hogging and sagging reinforcement for high reinforcement ratio ($\rho_{hogg} = 1{\cdot}5\%$), after yielding of hogging reinforcement for medium reinforcement ratio ($\rho_{hogg} = 0{\cdot}75\%$) and after yielding of hogging and sagging reinforcement for low reinforcement ratio ($\rho_{hogg} = 0{\cdot}375\%$). Even if not reported in the present study, it is important to observe that the sequence of events remains the same without considering shrinkage of concrete.

For fully externally restrained slabs, literature (Botte, 2017) reports that CMA decreases as the span length of the slab increases, while TMA is almost not affected by the span length. Figure 13 shows an opposite trend for self-restrained continuous slabs. In cases of high hogging reinforcement ratios ($\rho_{hogg} = 1{\cdot}5\%$), the peak value of CMA is similar for all values of analysed slenderness while the peak value of TMA is increasing as the span length is increasing. In cases of low hogging reinforcement ratios ($\rho_{hogg} = 0{\cdot}375\%$), the peak value of CMA is increasing as the slab slenderness is increasing, while the peak value of TMA is reaching an asymptotic value for all the analysed slenderness values.

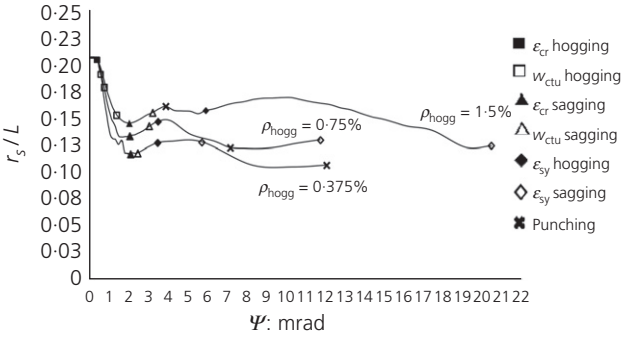

Figure 14. Variation of the point of contraflexure r_s as function of the rotation Ψ (case $c = 260$ mm, $h = 250$ mm, $L = 6$ m)

Moment redistribution effect on the point of contraflexure r_s

Figure 14 shows the variation of the point of contraflexure r_s with the slab rotation Ψ. Before cracking in the hogging area, the position of this point remains constant and corresponds approximately to $0{\cdot}22L$. After cracking of the hogging area, the position of the point of contraflexure r_s moves toward the column, reducing the effective slab slenderness r_s/d (Einpaul *et al.*, 2015, 2016).

This reduction continues till the maximum crack opening (w_{ctu}) in the hogging area is reached for a rotation Ψ approximately equal to 2 mrad for all the analysed slabs. The

Table 4. Assumptions for improved calculations according to LoA II and III

	CMA	Moment redistribution
Case A	Accounted for by calculating m_R on the basis of the radial stresses σ_{rad} (according to Figure 12)	Neglected (fixed value of r_s)
Case B	Neglected (m_R with $\sigma_{rad} = 0$)	Accounted for by varying the position of the point of contraflexure r_s (according to Figure 14)
Case C	Accounted for as in case A	Accounted for as in case B

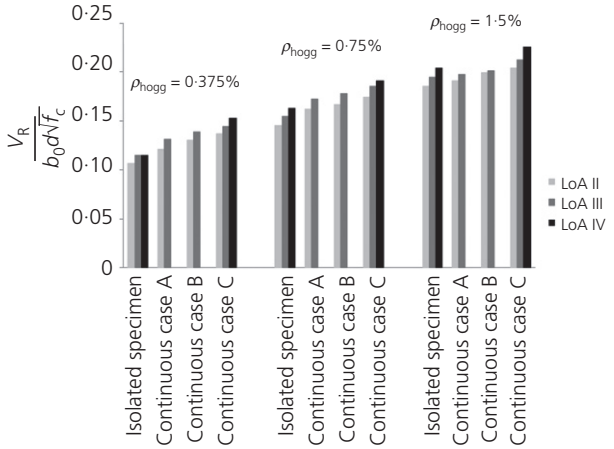

Figure 15. Comparison of the normalised punching shear resistance of an isolated specimen and a continuous slab (shrinkage neglected) where the LoA II and III are improved accounting for membrane effect (case A), moment redistribution (case B) and both effects (case C)

corresponding position of the point of contraflexure r_s depends on the hogging reinforcement ratios, with low values of r_s for low reinforcement ratios. Afterwards, an opposing trend is observed until yielding of hogging reinforcement occurs (when the position of the point of contraflexure r_s begins to move back to the column).

Punching shear resistance obtained using levels of approximation approach

The NLFEA described in the previous section shows that higher load-carrying capacities can be obtained in continuous flat slabs due to the membrane action in the column area (see compressive stresses in Figure 12) and moment redistributions leading to a variation of the effective slenderness expressed with parameter r_s (see Figure 14). Both effects can also be accounted for in an indirect manner in LoA II and LoA III approaches by adapting some parameters. The moment capacity m_R to be used in Equation 2 can be calculated while accounting for the radial stress σ_{rad} according to Figure 12 (on the basis of the calculated rotation Ψ), thus accounting indirectly for CMA. In a similar manner, the position r_s of the point of contraflexure, which is also an important parameter in Equation 2, can be taken from Figure 14, accounting for moment redistribution. This approach, which requires an iterative calculation as both parameters depend on rotation Ψ, allows for the separation of the influence of CMA and moment redistribution on the load-carrying capacity. At LoA II, $m_E = V_E/8$ is assumed, while at LoA III the average hogging moment is calculated on the basis of a linear elastic calculation.

To highlight the influence of both effects (membrane action and moment redistribution), the punching shear resistance obtained using LoA IV, which refers to NLFEA results, is compared to the resistances obtained with LoA II and LoA III with the three assumptions described in Table 4.

Figure 15 summarises the normalised punching shear resistances of an isolated specimen and a continuous slab (shrinkage neglected) where the LoA II and III are improved by accounting for membrane effect (Case A), moment redistribution (Case B) and both effects (Case C), as described in Table 4. It shows that analytical calculation of the punching shear resistance of continuous flat slabs carried out according to LoA II and LoA III is improved if membrane and moment redistribution effects are considered. Moment redistribution effects and the related variation of the position of the point of contraflexure r_s seem to be the predominant contribution to be considered to obtain resistances similar to NLFEA results (LoA IV).

Conclusions

This paper presents the results of a parametric study aiming to investigate the influence of different geometrical parameters (such as reinforcement ratios, column size, slab span and cover of the reinforcement) on the punching shear resistance of continuous flat slabs around internal columns without openings. The shrinkage effects on the punching shear resistance of RC flat slabs are also investigated.

The main conclusions are as follows.

- It is confirmed that the punching shear resistance of continuous flat slabs is higher than in equivalent isolated slabs. This is due to moment redistribution and CMA effects.
- The difference between the punching shear resistance of continuous slabs and the resistance of isolated slabs decreases as the hogging reinforcement ratio increases.

- Besides the effective depth, the total slab thickness also has a significant influence on the punching shear resistance. This parameter, which is usually neglected, has an influence on the effectiveness of the circular tie ring around the column, which provides confinement to the hogging area.
- Shrinkage of concrete leads to a reduction of the punching shear resistance. This effect is more pronounced for slabs with high reinforcement ratios where restrained deformations cause additional cracking and because failure occurs for lower deformation capacities.
- Due to nonlinear behaviour (cracking and yielding), the position of the point of contraflexure r_s varies with the slab rotation. The usually assumed value of $0{\cdot}22L$ (based on linear elastic calculations) leads to conservative results since radius values ranging from $0{\cdot}1L$ to $0{\cdot}16L$ have been calculated at failure. The value of r_s is smaller for low hogging reinforcement ratios since the effect of moment redistribution becomes more pronounced.
- Moment redistribution effects and the associated variation of the position of the point of contraflexure r_s seem to be the predominant effect compared to the CMA effect.
- In the framework of the LoA approach, better estimation of the punching shear resistance of continuous slabs can be achieved at LoA II or LoA III if parameters m_R and r_s are corrected accounting for CMA and moment redistribution.

REFERENCES

ACI (American Concrete Institute) (2014) ACI 318-14: Building code requirements for structural concrete and commentary. American Concrete Institute, Farmington Hills, MI, USA.

Amir S, Van Der Veen C, Walraven JC and De Boer A (2016) Experiments on punching shear behavior of prestressed concrete bridge decks. *ACI Structural Journal* **113(3)**: 627–636.

Arshian AH and Morgenthal G (2017) Probabilistic assessment of the ultimate load-bearing capacity in laterally restrained two-way reinforced concrete slabs. *Engineering Structures* **150**: 52–63.

Bailey CG (2001) Membrane action of unrestrained lightly reinforced concrete slabs at large displacements. *Engineering Structures* **23**: 470–483.

Belletti B, Cerioni R and Iori I (2001) Physical approach for reinforced-concrete (PARC) membrane elements. *Journal of Structural Engineering* **127(12)**: 1412–1426.

Belletti B, Esposito R and Walraven J (2013) Shear capacity of normal, lightweight, and high-strength concrete beams according to Model Code 2010. II: experimental results versus nonlinear finite element program results. *Journal of Structural Engineering* **139(9)**: 1600–1607.

Belletti B, Pimentel M, Scolari M and Walraven JC (2015a) Safety assessment of punching shear failure according to level of approximation approach. *Structural Concrete* **16(3)**: 366–380.

Belletti B, Walraven JC and Trapani F (2015b) Evaluation of compressive membrane action effects on punching shear resistance of reinforced concrete slabs. *Engineering Structures* **95(7)**: 25–39.

Belletti B, Damoni C, Cervenka V and Hendriks MAN (2016) Catenary action effects on the structural robustness assessment of RC slab strips subjected to shear and tensile forces. *Structural Concrete* **17(6)**: 1003–1016.

Belletti B, Scolari M and Vecchi F (2017) PARC_CL 2.0 crack model for NLFEA of reinforced concrete structures under cyclic loadings. *Computers and Structures* **191**: 165–179.

Bernardi P, Cerioni R, Michelini E and Sirico A (2016) Numerical simulation of early-age shrinkage effects on RC member deflections and cracking development. *Frattura ed Integrità Strutturale* **10(37)**: 15–21, https://doi.org/10.3221/IGF-ESIS.37.03.

Botte W (2017) *Quantification of Structural Reliability and Robustness of New and Existing Concrete Structures Considering Membrane Action*. PhD thesis, Ghent University, Ghent, Belgium.

Botte W, Gouverneur D, Caspeele R and Taerwe L (2014) Influence of design parameters on tensile membrane action in reinforced concrete slabs. *Structural Engineering International* **25(1)**: 50–60.

Botte W, Caspeele R and Taerwe L (2016) Membrane behavior in RC slabs subjected to simulated reinforcement corrosion. *Engineering Structures* **123**: 45–58.

Burgess I (2017) Yield-line plasticity and tensile membrane action in lightly-reinforced rectangular concrete slabs. *Engineering Structures* **138**: 195–214.

Cantone R, Belletti B, Manelli L and Muttoni A (2016) Compressive membrane action effects on punching strength of flat RC slabs. *Key Engineering Materials* **711**: 698–705.

CEN (European Committee for Standardization) (2004) EN 1992-1-1: Eurocode 2: Design of concrete structures – general rules and rules for buildings. CEN, Brussels, Belgium.

Clément T, Pinho Ramos A Fernández Ruiz M and Muttoni A (2014) Influence of prestressing on the punching strength of post-tensioned slabs. *Engineering Structures* **72**: 56–69.

Dat PX and Hai TK (2013) Membrane action of RC slabs in mitigating progressive collapse of building structures. *Engineering Structures* **55**: 107–115.

Di Prisco M, Martinelli P and Parmentier B (2016) On the reliability of the design approach for FRC structures according to fib Model Code 2010: the case of elevated slabs. *Structural Concrete* **17(4)**: 588–602.

Einpaul J, Ruiz MF and Muttoni A (2015) Influence of moment redistribution and compressive membrane action on punching strength of flat slabs. *Engineering Structures* **86**: 43–57.

Einpaul J, Ospina CE, Ruiz MF and Muttoni A (2016) Punching shear capacity of continuous slabs. *ACI Structural Journal* **113(4)**: 861–872.

fib (International Federation for Structural Concrete) (2013) *fib Model Code for Concrete Structures 2010*. fib, Lausanne, Switzerland.

Foster SJ, Bailey CG, Burgess IW and Plank RJ (2004) Experimental behaviour of concrete floor slabs at large displacements. *Engineering Structures* **26(9)**: 1231–1247.

Genikomsou AS and Polak MA (2017) 3D finite element investigation of the compressive membrane action effect in reinforced concrete flat slabs. *Engineering Structures* **136**: 233–244.

Gouverneur D, Caspeele R and Taerwe L (2013a) Experimental investigation of the load-displacement behaviour under catenary action in a restrained reinforced concrete slab strip. *Engineering Structures* **49**: 1007–1016.

Gouverneur D, Caspeele R and Taerwe L (2013b) Effect of reinforcement curtailment on deflections, strain and crack development in RC slabs under catenary action. *Magazine of Concrete Research* **65(22)**: 1336–1347.

Guidotti R (2010) *Poinçonnement des Planchers-Dalles avec Colonnes Superposées Fortement Sollicitées*. Doctoral thesis, EPFL, Lausanne, Switzerland (in French).

Kirkpatrick J, Rankin G and Long A (1986) The influence of compressive membrane action on the serviceability of beam and slab bridge decks. *The Structural Engineer* **64(13)**: 6–12.

Ladner M, Schaeidt W and Gut S (1977) *Experimentelle Untersuchungen an Stahlbeton-Flachdecke*. EMPA Bericht No. 205, Bauwesen und Gewerbe, Zurich, Switzerland (in German).

Manie J and Kikstra WP (eds) (2010) *DIANA Finite Element Analysis User's Manual: Material Library (Release 9.4.3)*. TNO DIANA BV, Delft, the Netherlands. See https://dianafea.com/manuals/d943/MatLib/MatLib.html (accessed 13/08/2018).

Muttoni A (2008) Punching shear strength of reinforced concrete slabs without transverse reinforcement. *ACI Structural Journal* **105**: 440–450.

Muttoni A, Fernández Ruiz M and Simões JT (2018) The theoretical principles of the critical shear crack theory for punching shear failures and derivation of consistent closed-form design expressions. *Structural Concrete* **19**: 174–190, https://doi.org/10.1002/suco.201700088.

Park R and Gamble WL (2000) *Reinforced Concrete Slabs*, 2nd edn. John Wiley, New York, NY, USA.

Qian K, Li B and Zhang Z (2015) Testing and simulation of 3D effects on progressive collapse resistance of RC buildings. *Magazine of Concrete Research* **67(4)**: 163–178.

Rankin GIB and Long AE (1997) Arching action strength enhancement in laterally restrained slab strips. *Proceedings of the Institution of Civil Engineers – Structures and Buildings* **122(4)**: 461–467.

Shu J, Belletti B, Muttoni A, Scolari M and Plos M (2017) Internal force distribution in RC slabs subjected to punching shear. *Engineering Structures* **153**: 766–781.

Simões JT, Fernández Ruiz M and Muttoni A (2018) Validation of the Critical Shear Crack Theory for punching of slabs without transverse reinforcement by means of a refined mechanical model. *Structural Concrete* **19**: 191–216.

Soares LFS and Vollum RL (2015) Comparison of punching shear requirements in BS 8110, EC2 and MC2010. *Magazine of Concrete Research* **67(24)**: 1315–1328.

Soares LFS and Vollum RL (2016) Influence of continuity on punching resistance at edge columns. *Magazine of Concrete Research* **68(23)**: 1225–1239.

Taylor SE, Rankin B, Cleland DJ and Kirkpatrick J (2007) Serviceability of bridge deck slabs with arching action. *ACI Structural Journal* **104(1)**: 39–48.

Wood RH (1961) *Plastic and Elastic Design of Slabs and Plates, with Particular Reference to Reinforced Concrete Floor Slabs*. Thames and Hudson, London, UK.

Wu HQ and Gilbert RI (2008) *An Experimental Study of Tension Stiffening in Reinforced Concrete Members under Short-Term and Long-Term Loads*. University of New South Wales, Sydney, NSW, Australia.

Zeng Y, Caspeele R, Matthys S and Taerwe L (2016) Compressive membrane action in FRP strengthened RC members. *Construction and Building Materials* **126**: 442–452.